Eur. Phys. J. B **5**, 143–152 (1998)

THE EUROPEAN PHYSICAL JOURNAL B

© EDP Sciences
Springer-Verlag 1998

General plasma behavior in the energy relaxation of electrons in highly p-doped semiconductors*

U. Hohenester[1a], P. Kocevar[2], N.E. Hecker[3], and R. Rodrigues–Herzog[4]

[1] Istituto Nazionale per la Fisica della Materia (INFM) and Dipartimento di Fisca, Università di Modena, 41100 Modena, Italy
[2] Institut für Theoretische Physik, Karl–Franzens–Universität Graz, 8010 Graz, Austria
[3] Institut für Experimentalphysik, Universität Innsbruck, 6020 Innsbruck, Austria
[4] Département de Chimie Physique, Université de Genève, 1211 Geneva and Institut für Physik, Universität Basel, 4056 Basel, Switzerland

Received: 1st April 1998 / Revised: 6 May 1998 / Accepted: 18 May 1998

Abstract. We present a systematic study of the dependence of the energy relaxation of photo-excited minority electrons on the doping concentration in highly p-doped GaAs. A nonmonotonic dependence is found in the region where the characteristics of the carrier-carrier interaction changes from plasmon-mediated to quasistatically screened. Using a detailed Monte-Carlo study we are able to attribute this observation to a general property of plasmas at high density.

PACS. 78.47.+p Time-resolved optical spectroscopies and other ultrafast optical measurements in condensed matter – 72.20.Jv Charge carriers: generation, recombination, lifetime, and trapping – 71.10.Ca Electron gas, Fermi gas

1 Introduction

The role of carrier–carrier collisions in the energy-loss dynamics of nonequilibrium carrier plasmas at high density has recently been a topic of intense research, both in metals [1–5] and p-doped semiconductors [6–11]. Despite the intrinsic differences between these two types of materials the physics underlying such transport problems is remarkably similar. This may seem, at first, somewhat surprising since the free-carrier densities of metals ($\sim 10^{23}$ cm^{-3}) and of even highly doped semiconductors ($p \sim 10^{18}$–10^{19} cm^{-3}) differ by more than four to five orders of magnitude. However, it is well known that the relevant quantity in the description of free-carrier plasmas is the ratio of the mean distance between electrons and the effective Bohr radius [12], rather than just the interparticle distance. The difference in density between metals and semiconductors is thus almost compensated by the larger effective Bohr radius in semiconductors, due to the smaller effective hole mass, m_h, and the larger background dielectric constant, ϵ_∞ (*e.g.*, $m_h \simeq 0.38 m_o$ and $\epsilon_\infty = 10.92$ for GaAs).

Recently, we have reported the observation of a decrease in the energy-loss rate of photo-excited minority electrons in p-type GaAs at doping levels above $p \geq 2 \times 10^{19}$ cm^{-3} [11]. We have attributed this behavior of the energy transfer to a transition from dominant plasmon-mediated, at low densities, to free-carrier-screened electron-hole scattering, at high densities. In the present paper we examine this problem by means of detailed Monte-Carlo studies and provide further theoretical evidence that such a nonmonotonic behavior of the energy-loss rate as a function of doping is indeed a general property of plasmas at high carrier density.

Besides their important technological applications [8], highly p-doped semiconductors offer the opportunity to address some interesting fundamental questions. First, they enable us to study the energy-loss dynamics of minority carriers (*i.e.*, electrons) in a system where one can *vary the background density of majority carriers while at the same time keeping all other material parameters fixed.* This differs appreciably from related studies in metals where the density can solely be "changed" by comparing different materials with their intrinsically different band structures. We also stress that additional details of the scattering dynamics (*e.g.*, electron-phonon couplings) are much less known in metals than in semiconductors. The second reason for our analysis is related to the lack of a rule-of-thumb for the density dependence of the energy-loss rates due to carrier-carrier collisions in plasmas of high density. Quite generally, one expects that with increasing density the carrier-carrier scattering rates should (i) increase due to the larger number of scattering partners, but (ii) decrease due to more efficient screening. In addition, one also has to consider (iii) the mean energy exchanged in a single scattering event, (iv) the role of

* Dedicated to Ralph A. Höpfel (1955–1997)

[a] e-mail: `hohenester@unimo.it`.

degeneracy, and (v) the influence of temperature. In light of all these points, it may seem surprising that there exists, as discussed in more detail in Sections 3 and 4, a simple rule for the density dependence of the energy-loss rate, which depends only on the mean excess energy of the minority carriers, $\langle E \rangle$, and the plasmon energy of the majority carriers, E_{pl}. For systems with a given mean excess energy $\langle E \rangle$ the energy loss as a function of density depicts a maximum around the density where the corresponding plasmon energy E_{pl} equals $\langle E \rangle/2$.

We have organized our paper as follows. In Section 2 we present the results of our experiments. Our theoretical framework is presented in Section 3; in particular, we discuss the energy loss of one energetic electron to a cold doping background of carriers and present the ingredients of our Ensemble-Monte-Carlo simulations. Their results will be discussed in Section 4. We finally draw some conclusions in Section 5.

2 Experiments

In the experiments we used six p-type GaAs samples with doping concentrations of $p = 1 \times 10^{18}$ cm^{-3} (sample A), 1×10^{19} cm^{-3} (sample B), 1.8×10^{19} cm^{-3} (sample C), 1.9×10^{19} cm^{-3} (sample D), 2.7×10^{19} cm^{-3} (sample E), and 4×10^{19} cm^{-3} (sample F). At such high doping levels, impurity banding is expected to dominate over any bound hole contributions [13,14] (with the possible exception of the moderately doped sample A). This is also confirmed by our complementary Hall data for samples D and F which show a negligible temperature dependence between 10 and 300 K. Since the modification of the density of states due to impurity banding only influences states at the bottom of the band, which are of minor importance for the energy loss dynamics of our present concern, we conclude that a variation of doping levels solely changes the concentration of background carriers without influencing the essentials of the band structure.

The energy loss of minority electrons was investigated using femtosecond luminescence spectroscopy [15]. Electron-hole pairs were generated through an ultrashort laser pulse (pulse duration of $\approx$ 80 fs), and their ensuing relaxation was monitored by measuring the time- and frequency–resolved luminescence. In order to obtain a time resolution below 100 fs, we used the upconversion technique [16]. The peak of the excitation wavelength was varied between 738 and 800 nm (*i.e.*, photon energies of 1.68–1.55 eV) to keep the excess energy of the photoexcited electrons far below the GaAs satellite valleys. For all doping levels the excess energy was $\approx$ 120 meV [17]. Our measurements were performed at 77 K (with the only exception of the room-temperature data shown in Fig. 2).

The extremely fast dephasing process of free carriers in the case of dominant carrier-carrier scattering (phase relaxation time $\tau_p \sim 10$ fs [18]) then allows a direct description of the luminescence spectra through carrier distribution functions. The luminescence intensity corresponding to the optical transition energy $h\nu$ at time t is given by a

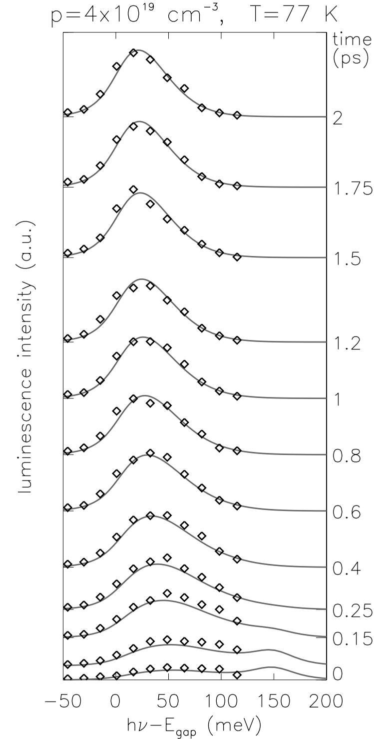

Fig. 1. Luminescence spectra for sample F at different delay times (see right axis) at 77 K. The diamonds are the experimental data; the solid lines are the results of our Monte-Carlo simulations.

sum over the heavy- and light-hole contributions [19]:

$$I_{lum}(h\nu, t) \propto (h\nu)^2 \sum_{h=hh,lh} |H_{opt}^{(h)}|^2 \rho(h\nu) \times f_e(E_e^{(h)}, t) f_h(E_h^{(h)}, t), \quad (1)$$

where $f_e(E_e^{(h)}, t)$ and $f_h(E_h^{(h)}, t)$ are the electron and hole distribution functions at the corresponding transition energies, $H_{opt}^{(h)}$ is the optical transition matrix element, and $\rho(h\nu)$ the joint density of states. Since in our experiments we worked with low excitation densities ($N_{exc} \approx 1 \times 10^{17}$ cm^{-3}) as compared to the high doping concentrations, the hole distributions remained practically at equilibrium and therefore constant over time. As a consequence, the temporal evolution of the luminescence was exclusively determined by the time evolution of the electron distribution function. Thus, femtosecond spectroscopy and the use of differently p-doped semiconductor samples allows the systematic investigation of the energy relaxation of minority electrons within a wide range of different energies and doping levels.

The diamonds in Figure 1 show the measured luminescence spectra for our highest doped sample at 12 characteristic delay times at a lattice temperature of 77 K. Nonthermal features are not present in the observed spectra, indicating that thermalization occurs on the time scale of our experimental resolution (< 100 fs). Because

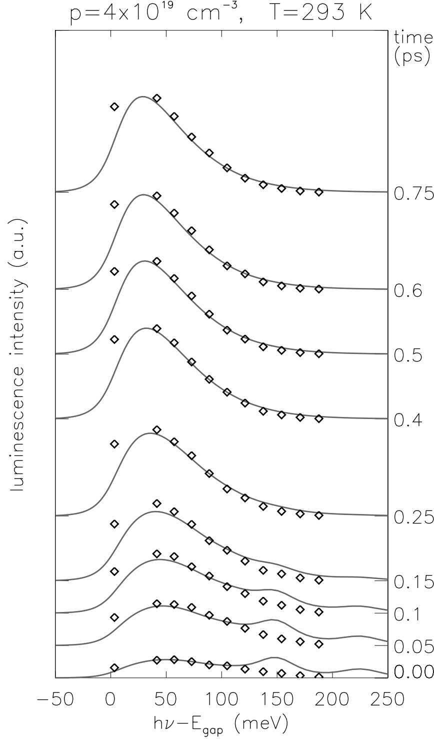

Fig. 2. Luminescence spectra for sample F at different delay times (see right axis) at room temperature. The diamonds are the experimental data (taken from Ref. [20]); the solid lines are the results of our Monte-Carlo simulations.

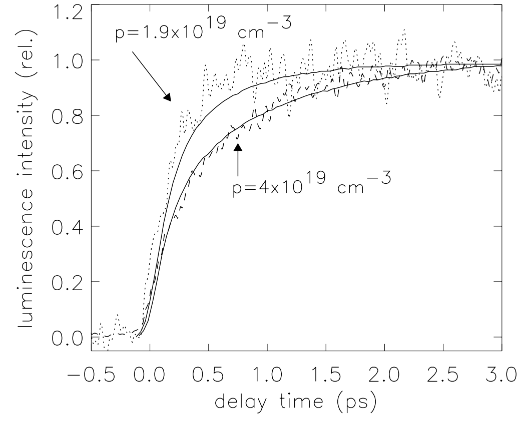

Fig. 3. Time evolution of the luminescence intensity at 13 meV above the renormalized band edge for sample D ($p = 1.9 \times 10^{19}$ cm^{-3}) and sample F ($p = 4 \times 10^{19}$ cm^{-3}) at the lattice temperature of 77 K. The solid lines show the results of the Monte-Carlo simulations.

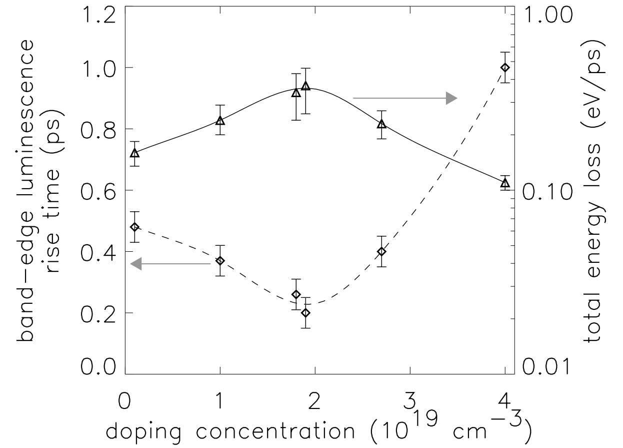

Fig. 4. Band-edge luminescence rise time (left axis) and corresponding average of the total energy loss rate of electrons as defined in the text (right axis) *vs.* doping concentration. The solid and dashed lines are only to guide the eye.

our present experimental setup can only detect the luminescence from photons with a photon energy below ~ 1.550 meV (*i.e.*, at 77 K from band regions below photogeneration) we also analyzed luminescence spectra taken at room temperature, where luminescence from the region of photoexcitation can be observed since the fundamental bandgap decreases with increasing temperature. Figure 2 shows the transient luminescence spectra for the $p = 4 \times 10^{19}$ cm^{-3} sample at room temperature. It can be seen that the luminescence spectra show *no nonthermal features even during photoexcitation*. This is a remarkable result since thermalization appears to be almost instantaneous. Our observed fast thermalization on the time scale of the experimental resolution is also in agreement with earlier measurements [21] at similar excitation densities, and is further supported by our theoretical analysis given in Section 4.1.

Effects of electron degeneracy are of minor importance at our low excitation densities. For a preliminary analysis of our data, the electron distribution function f_e can (at times later than ~ 100 fs) thus be well approximated by an internally thermalized Maxwell distribution with a transient temperature $T_e(t)$ and a corresponding mean electron energy $\langle E_e \rangle(t) = 3k_B T_e(t)/2$, where k_B is Boltzmann's constant. From equation (1) we see that the luminescence intensity for a given photon energy is then an extremely sensitive measure of the transient electron mean energy.

Figure 3 shows the onset of the experimentally observed luminescence intensity at the luminescence maximum, *i.e.*, ≈ 13 meV above the calculated band edge, for samples D ($p = 1.9 \times 10^{19}$ cm^{-3}) and F ($p = 4 \times 10^{19}$ cm^{-3}). The rise time for the highest doped sample F is clearly *slower* than that for the sample with the lower doping concentration [22]. Figure 4 shows the experimental band-edge luminescence rise time (left axis) *versus* doping concentration, as obtained from the six samples. Here the rise time is defined as the time it takes for the luminescence to reach 75% of its maximum value, with the time zero taken at the center of the excitation pulse. A clear minimum is observed in the vicinity of a doping concentration of $p \approx 2 \times 10^{19}$ cm^{-3}.

In order to determine the energy-loss rate as a function of the doping density, we analyzed the time interval in which the band-edge luminescence increases to 75% of its maximum value. Using in equation (1) a heated Maxwellian f_e and a frequency convolution of 35 meV to account for the spectral laser width and the experimental spectral resolution, we then obtain $T_e(t)$ as a function of the measured band-edge luminescence intensity. Thus, 75% of the maximum band-edge luminescence corresponds to an average electron energy of approximately 17 meV ($T_e \approx 130$ K) for all investigated densities, whereas the initial excess energy of the photoexcited electrons is $\approx$ 120 meV. We note that these estimates do not depend decisively on the details of the underlying band-structure description. The averaged energy-loss rate, which is defined as the difference between the initial excess energy and 17 meV divided by the band-edge luminescence rise time, is shown in Figure 4 (right axis). The cooling rate exhibits a maximum at the majority hole concentration of $p \approx 2 \times 10^{19}\mathrm{cm}^{-3}$; at higher doping concentrations it dramatically decreases.

3 Theoretical model

It is well known from related earlier work that electron-hole scattering is the dominant energy-loss channel for minority electrons at high doping levels [7–10,23]. For this reason we shall now investigate the electron-hole interactions in more detail. Our theoretical analysis is based on the semiclassical Boltzmann equation. Electron-hole scatterings are described within the random-phase approximation (RPA). In view of the longstanding and successful application of the RPA in semiconductor transport (see, *e.g.*, Ref. [15]) we think that our present theoretical framework, despite its limitations, can be considered as a first and sound approximation.

As a preliminary simplification we address in Section 3.1 solely the energy loss of *one* energetic electron to a doping background of holes in p-type GaAs and compare these results with those of conventional electron-gas theory in Section 3.2. The ingredients of our complete Monte-Carlo simulations will then be presented in Section 3.3.

3.1 Energy loss of one energetic electron in p-type GaAs

The total electron-hole scattering rate for an energetic electron with wavevector $\mathbf{k}$ and energy $\varepsilon_e(\mathbf{k})$ interacting with a doping background of holes is given within the RPA by [24,25]:

$$\mathcal{P}_{\mathrm{eh}}(\mathbf{k}) = \int_{-\infty}^{\varepsilon_e(\mathbf{k})} d\omega \sum_{\mathbf{q}} 2\pi |v_s(\mathbf{q},\omega)|^2 (1 - f_e(\varepsilon_e(\mathbf{k}) - \omega)) \times S_o(\mathbf{q},\omega)\delta(\omega + \omega_{ee}(\mathbf{k},-\mathbf{q})), \qquad (2)$$

where $\omega_{ij}(\mathbf{k},\mathbf{q}) = \varepsilon_j(\mathbf{k}+\mathbf{q}) - \varepsilon_i(\mathbf{k})$; we set $\hbar = 1$. Here, the dynamic form factor S_o consists of intra- and inter-valence band contributions,

$$S_o(\mathbf{q},\omega) = 2 \sum_{\mathbf{k}',hh'} \mathcal{G}_{hh'}(\mathbf{k}',\mathbf{k}'+\mathbf{q}) f_h(\varepsilon_h(\mathbf{k}')) \times (1 - f_{h'}(\varepsilon_{h'}(\mathbf{k}') + \omega))\delta(\omega - \omega_{hh'}(\mathbf{k}',\mathbf{q})), \qquad (3)$$

where $\mathcal{G}$ denotes the overlap factor[26,24]. Finally,

$$v_s(\mathbf{q},\omega) = \frac{v(q)}{\epsilon_{\mathrm{RPA}}(\mathbf{q},\omega)} \qquad (4)$$

$$\epsilon_{\mathrm{RPA}}(\mathbf{q},\omega) = 1 - v(q)P(\mathbf{q},\omega) \qquad (5)$$

$$v(q) = \frac{4\pi e^2}{\epsilon_\infty q^2}, \qquad (6)$$

with e the elementary charge and ϵ_∞ the optical dielectric constant. Here, the polarization P is related to the dynamic form factor through

$$P(\mathbf{q},\omega) = \int \frac{d\omega'}{2\pi} \frac{S_o(\mathbf{q},\omega') - S_o(-\mathbf{q},-\omega')}{\omega - \omega' + i0^+}, \qquad (7)$$

where the infinitesimally small quantity 0^+ ensures causality.

In the computational treatment of the electron-scattering rates of equation (2), several points are worth emphasizing: (i) since in our experiments the electron excitation energies were of the order of the plasmon energies E_{pl} of the doping background the use of the *full* dielectric function (Eq. (5)) turned out to be of crucial importance; (ii) because E_{pl} was of the order of the average energy separation between the heavy-hole and light-hole valence band, we had to go beyond the simple parabolic valence-band model to provide an accurate description of plasmon-induced inter-valence band transfers in upper band regions.

In the treatment of the valence-band structure, modifications of the density of states (DOS) due to impurity banding were neglected, since such details would only influence states at the bottom of the bands, which are of minor importance for the present energy-loss analysis. The nonparabolicities in the bandstructure were then treated within an 8×8 $\mathbf{k}\cdot\mathbf{p}$ model [27]. In order to obtain computationally simpler expressions we did not take the full details of the valence-band structure into account, but performed an average of $\varepsilon_h(\mathbf{k})$ over all angles. We furthermore assumed that the overlap factors for holes $\mathcal{G}_{hh'}$ depend only on the modulus of the initial wavevector k and the cosine of the angle θ between the initial and final wavevector, *i.e.*, $\mathcal{G}_{hh'}(\mathbf{k},\mathbf{k}') \cong \mathcal{G}_{hh'}(k,\cos\theta)$. The latter assumption is inspired by Wiley's approximation for $\mathcal{G}$ [28]. In our calculations we checked Wiley's approximation against ours, finding no significant difference.

The calculation of the dynamic form factor S_o and of the imaginary part of the polarization P (see Eqs. (3) and (7)) reduces, due to our use of a directionally averaged band structure, to two-fold integrals, which were solved by storing S_o and P in an equidistant array (with a typical size of 80×80) and performing linear interpolation

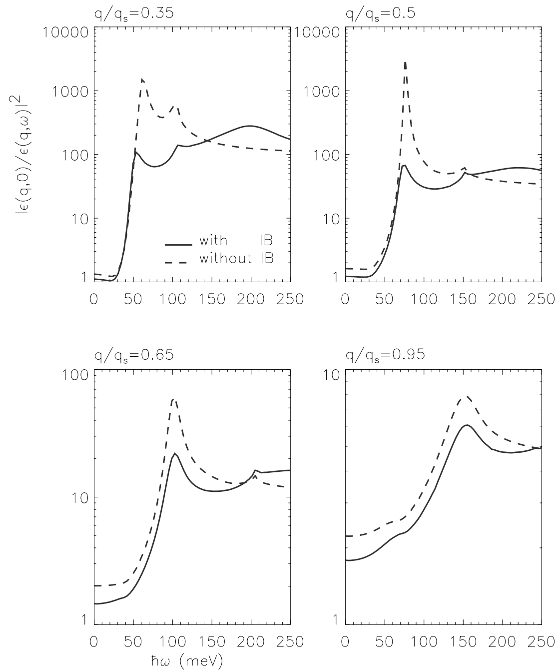

Fig. 5. Enhancement of the electron-hole scattering rates (Eq. (2)) due to dynamic screening for a doping background of $p = 2 \times 10^{19}$ cm^{-3} at 77 K. The influence of the intervalence-band contributions (IB) to the dielectric function can be seen from the difference of the two curves.

between mesh points. The computation of the real part of the polarization then invokes the use of the Kramers-Kronig relation (through Eq. (7)). In general, rather large integration limits of $\sim \pm 300$ meV were required to recover the static dielectric function in the low-frequency limit. Finally, in the computation of the electron-hole scattering rates of equation (2) particular attention had to be paid to the strong enhancement of the integrand at the zeroes of Re $\epsilon_{\mathrm{RPA}}(\mathbf{q}, \omega)$ (plasmon pole), which were treated by use of a Runge-Kutta algorithm with adaptive step size.

Figure 5 shows the dynamic enhancement factor $|\epsilon(q,0)/\ \epsilon(q,\omega)|^2$ in the scattering rates of equation (2) for different wavevectors q (in units of the static screening wavevector q_s, as given by the static long-wavelength limit of the RPA dielectric function of equation (5)) for a hole concentration $p = 2 \times 10^{19}$ cm^{-3} at 77 K. The two peaks of the enhancement factor can be attributed (*i*) to the plasmon resonance and (*ii*) to the (single-particle) intra- and inter-valence-band transitions in the dynamic form factor of equation (3) [24]. In particular, one observes that the $hh \leftrightarrow lh$ contributions to $\epsilon_{\mathrm{RPA}}(q,\omega)$ lead to a strong damping of the plasmon resonance [29,24].

The energy loss rate of one energetic electron with a kinetic energy E_{ini} to a doping background of holes in p-type GaAs at a lattice temperature of 77 K is shown in Figure 6a (the doping concentrations of $p = 1 \times 10^{18}$ cm$^{-3}, 1 \times 10^{19}$cm^{-3}, and 2×10^{19} cm^{-3} correspond to plasmon energies of $\approx$ 26, 58, and 82 meV, respectively). Quite generally, it turns out that in the energy-loss dynamics three different regimes can be distinguished which are determined by the ratio of the excess energy E_{ini} and the plasma frequency E_{pl} [31]: (*i*) the low-excitation regime with $E_{ini} \ll E_{pl}$, (*ii*) the high-excitation regime with $E_{ini} \gg E_{pl}$, and (*iii*) the intermediate region. Below the threshold of plasmon emission, *i.e.*, in the low-excitation regime, the electron loses energy through statically screened individual particle collisions, whereas for $E_{ini} \gg E_{pl}$ the electron relaxes predominately via plasmon emissions. In the intermediate region, *i.e.*, for $E_{ini} \approx E_{pl}$, the electron suffers individual collisions where the scattering rates are strongly enhanced when the exchanged energy is of the order of the plasmon energy, $\omega \approx E_{pl}$ (see also Fig. 5); for this reason we shall characterize this intermediate regime as *plasmon-mediated*. We shall find it useful to adopt this notation throughout [30].

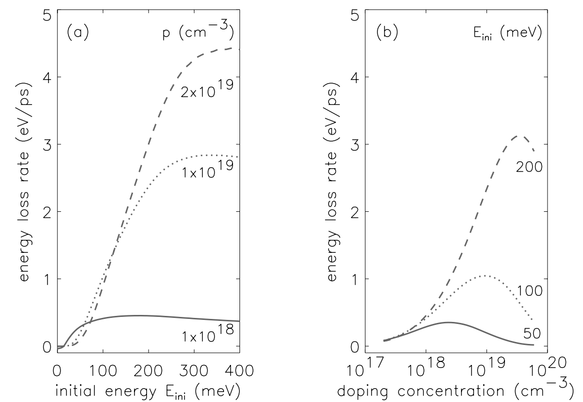

Fig. 6. Energy-loss rate of an energetic electron in p-type GaAs at 77 K as a function: (a) of the initial energy E_{ini} for three different doping levels (right axis); (b) of the doping concentration for three different initial energies (right axis).

We can investigate the same problem from a different point of view by fixing the initial energy and varying the doping levels, as depicted in Figure 6b. Such an investigation reveals, in particular, the dependence of the energy loss on doping. We find that (i) in the low-excitation regime, *i.e.*, at high doping levels, the energy loss rate $\dot{E}_{ini}$ *decreases* with increasing density due to the more efficient static screening (through cold background holes) of the individual scattering events, whereas (ii) in the high-excitation regime, *i.e.*, at low doping levels, $\dot{E}_{ini}$ *increases* with increasing density due to the increasing plasmon energies and plasmon emission rates. The intermediate region then displays a maximum.

Figure 7 shows the doping concentrations where the energy-loss rate $\dot{E}_{ini}(p)$ is maximal for different E_{ini} (left axis). Relating the maximum of $\dot{E}_{ini}$ to the plasma frequency E_{pl} (right axis of Fig. 7) rather than to p, we observe that the energy loss is maximal at densities *where the plasmon energy* $E_{pl}(p)$ *is approximately half the excess energy* E_{ini}. This behavior persists over a large range of densities. This is a remarkable result. As can be inferred from Figure 8, showing the hole distribution function f_h for different doping levels, the relation $E_{pl,max}(p) \approx E_{ini}/2$ prevails in Figure 7 over two orders of magnitude in the

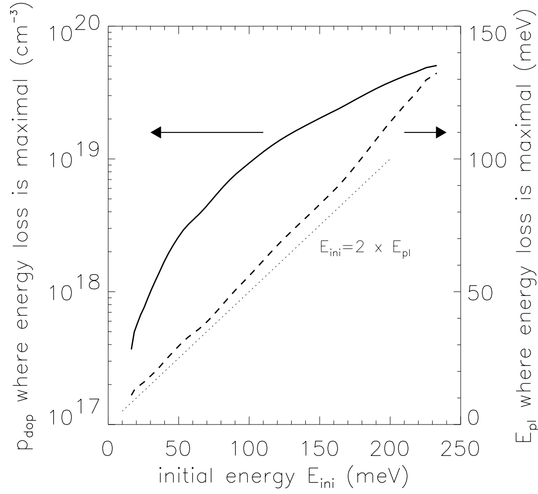

Fig. 7. Doping concentration (left axis) and plasmon energy $E_{pl,max}$ (right axis) where energy-loss rate is maximal for a given initial energy E_{ini}. The temperature of the doping background is 77 K.

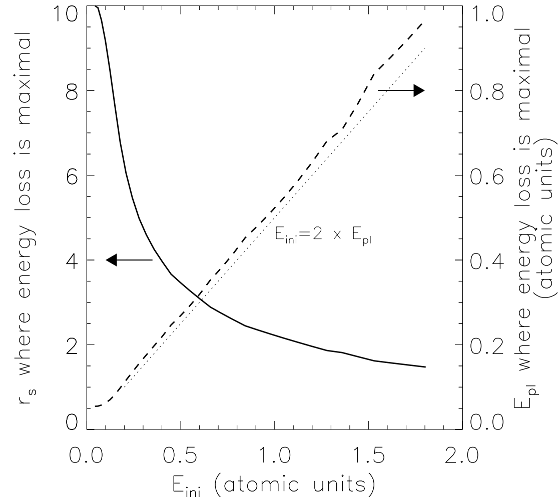

Fig. 9. Electron-gas parameter r_s (left axis) and plasmon energy E_{pl} (right axis) where energy-loss rate is maximal for a given excess energy $E_{ini} = E - E_F$.

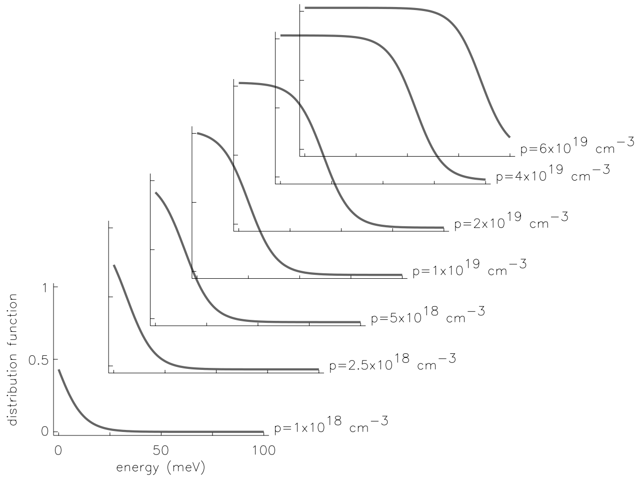

Fig. 8. Hole distribution function in p-GaAs at 77 K for different doping concentrations.

doping level within which f_h changes from a non-degenerate to a highly degenerate distribution. Because of this, we conclude that the existence of a maximum of $\dot{E}_{ini}(p)$ is mainly caused by the change of the characteristics of the electron-hole scatterings from statically screened to plasmon mediated. Degeneracy of the hole distributions, although being essential for a proper description of the energy-loss dynamics of the energetic electron, has no significant influence on the position of the maximum.

3.2 Energy loss of one energetic electron in an electron gas at zero temperature

The discussion of the preceding section has indicated that the existence of a maximum of the energy-loss rate as a function of background density and its relation to the plasmon energy are general properties of plasmas at high density. To provide further support for this conclusion, we devote this section to a short discussion of the energy loss of *one* energetic electron to an electron gas at zero temperature. The electron-gas can be considered as "the prototype" of an idealized high-density plasma and is among the systems most thoroughly studied theoretically. For these reasons we think that such a discussion could substantially elucidate the analysis presented in Section 3.1.

The electron-gas theory describes a system of interacting electrons moving in a homogeneous positively charged background. Defining, as usual, a length scale r_s in terms of the volume per particle:

$$n^{-1} = \frac{4}{3}\pi r_s^3, \tag{8}$$

where n is the density of electrons (in this section we use atomic units, *i.e.*, distances are measured in units of the Bohr radius and energies in units of Hartree (two Rydbergs)) we obtain, within the random-phase approximation, for the probability per unit time that an additional electron transfers momentum $\mathbf{q}$ and energy ω to the electron gas, the well-known result [12]:

$$\mathcal{P}(\mathbf{q},\omega) = \frac{8\pi}{q^2}\Im\left(-\frac{1}{\epsilon_{\mathrm{RPA}}(\mathbf{q},\omega)}\right), \tag{9}$$

with Lindhard's dielectric function $\epsilon_{\mathrm{RPA}}(\mathbf{q},\omega)$.

Figure 9 depicts the values r_s where the total energy-loss rate $\dot{E}_{ini}(r_s)$, derived from equation (9), is maximal for different excess energies $E_{ini} = E - E_F$ above the Fermi energy E_F. Relating the maximum of $\dot{E}_{ini}$ to the plasma frequency E_{pl} (right axis of Fig. 9) rather than to r_s, we observe, once again, that the energy loss is maximal at densities *where the plasmon energy $E_{pl}(r_s)$ is approximately half the excess energy E_{ini}.*

This is an important result since the electron gas appreciably differs from the doping background in p-type GaAs (one electron band with a parabolic dispersion and an electron distribution at zero temperature *vs.* different valence bands with a nontrivial dispersion and a doping distribution at finite temperature) while the trends of the energy loss of one energetic carrier to these plasmas are surprisingly similar. For this reason, we conclude, that the relation between the maximum of the energy-loss rate as a function of the particle density of the cooling agent and the corresponding plasmon energy is a general property of plasmas whose dynamics is dominated by carrier-carrier interactions.

3.3 Monte-Carlo simulations

Our detailed theoretical analysis of the experiments is based on the semiclassical Boltzmann equation, which was solved by use of the Ensemble-Monte-Carlo (EMC) technique [26]. Since the technical details of our EMC approach have been presented elsewhere [10] we only emphasize the novel features (see also Sect. 3.1) namely (i) the use of a fully dynamical screening model, (ii) the inclusion of nonparabolicities in the valence-band structure, and (iii) our explicit treatment of hole-degeneracy in the evaluation of the scattering rates of equation (2) rather than making use of the usual Monte-Carlo rejection technique [26]. Since in our experiments the doping concentrations were much larger than the excitation densities the hole distributions remained practically at equilibrium. Therefore, we neglected deviations of the hole distributions from equilibrium. Furthermore, contributions of photoexcited carriers to the dielectric function $\epsilon_{RPA}(\mathbf{q},\omega)$ are assumed to be of minor importance and were not taken into account. These approximations strongly simplified our computational approach, because the electron-hole scattering rates of equation (2) needed to be computed only once. We finally treated electron degeneracy through the usual EMC rejection technique and described electron-phonon scatterings within a static screening model. Effects of hot phonons were neglected.

In our simulations we used (i) an excess energy $h\nu - E_{gap}$ of 230 meV, (ii) a spectral laser width $\Delta h\nu$ of 20 meV, (iii) a temporal halfwidth of 80 fs, and (iv) an excitation density of $N_{exc} = 5 \times 10^{16}$ cm^{-3}. A temporal convolution of 80 fs was performed in the calculated luminescence spectra of equation (1), together with a frequency convolution of 35 meV at 77 K (25 meV at room temperature) to account for the spectral laser width in the up-conversion and for the experimental spectral resolution.

4 Results and discussion

4.1 Thermalization

Figure 10 shows the temporal evolution of the calculated electron distribution function f_e at three doping concentrations and at 77 K for an 80 fs excitation pulse. At early times we observe the excitation peaks from the light- and heavy-hole channels at electron excess energies of ≈ 130 and ≈ 200 meV, respectively. The hh-channel becomes more and more blocked at higher doping concentrations due to the increasing degeneracy of the hole distributions (see also Fig. 8). A striking feature of our simulations is that electron states near the band minimum are populated already during the photoexcitation due to extremely efficient plasmon-mediated electron-hole scatterings.

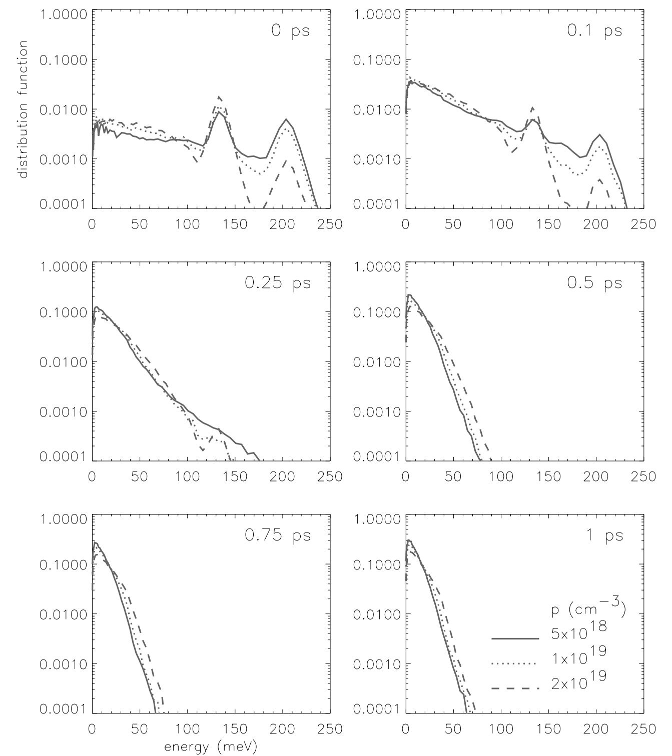

Fig. 10. Temporal evolution of the electron distribution function f_e at six different delay times for three different doping concentrations and $T = 77$ K.

From Figure 10 we observe that during the first 200 fs nonthermal features practically disappear (this process is usually called *thermalization*), and that immediately after (and during) photoexcitation the electron distribution at energies below 100 meV can be described by an internally thermalized Boltzmann distribution $\exp(-E_e/k_B T_e)$. Effects of degeneracy in the conduction band are of minor importance throughout. However, the persistence of photoexcitation peaks up to an order of 200 fs seems to be somewhat surprising in view of earlier results of similar studies [21,10], which reported thermalization times below 100 fs. The nonthermal features of our present simulations also show up in the calculated luminescence spectra of Figures 1 and 2, in contrast to the experiments where thermalization appears to be almost instantaneous. We attribute this systematic discrepancy between the experimental data and the results of our simulations to (i) our neglect of the interplay of scatterings with the coherent excitation dynamics [32,33], which should lead to an additional broadening during photoexcitation, (ii) the possible higher excitation densities in the experiments, and

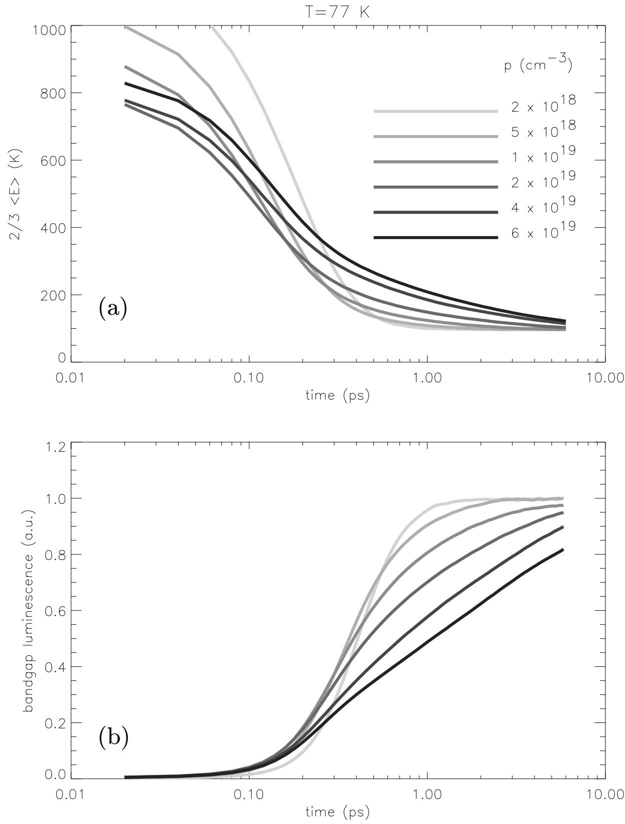

Fig. 11. (a) Electron "temperature" $T_e(t) = 2/3\langle E_e \rangle(t)$ (K) as a function of time for six differently p-doped semiconductors at 77 K for an 80 fs laser pulse. (b) Corresponding transient band-edge luminescence.

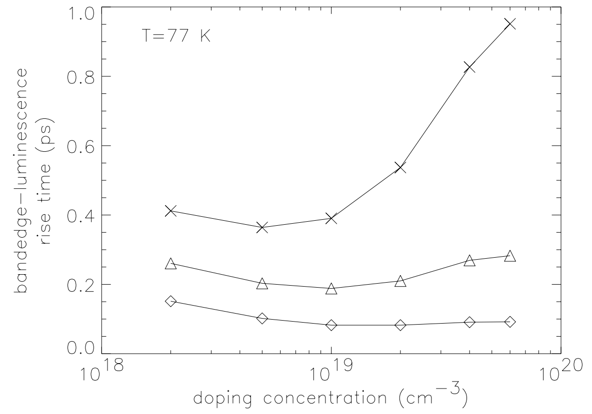

Fig. 12. Doping dependence of the calculated BEL rise times to 25% (◇), 50% (△), and 75% (×) of the respective asymptotic BEL intensities.

(*iii*) possible effects of impurity banding. Point (*i*), in particular, indicates the limitations of our present use of the semiclassical Boltzmann description and shows that a more refined treatment of the carrier dynamics is required for an accurate description at the earliest times [32]. Nevertheless, with the exception of these nonthermal features at times below ≈ 200 fs the experimental and theoretical luminescence spectra (Figs. 1 and 2; see also Fig. 3) are in very good agreement at both 77 K and room temperature. Thus, we assume that our theoretical model contains all relevant ingredients necessary to provide a proper description of the energy loss dynamics of the minority electrons under the present experimental conditions.

We finally note that in Figure 10 two slopes can be observed in the logarithmic plot of the electron distribution function at times later than ~ 0.5 ps. This effect can be attributed to the threshold of LO-phonon emission causing a faster energy loss of carriers above threshold.

4.2 Band-edge luminescence

The discussion of the preceding section has confirmed our initial assumption in Section 2 that at times ≥ 100 fs the electron distribution can be well described by an internally thermalized Maxwellian. We stress that in our simulations we did *not* make any assumption about the particular shape of f_e. Figure 11 shows $T_e(t) = 2/3\langle E_e \rangle(t)$ (a) and the corresponding transient band-edge luminescence (b) for different doping concentrations at 77 K. Here the band-edge luminescence (BEL) is taken for each doping concentration at the energy of the maximum of the asymptotic luminescence spectra (see also Fig. 3).

Figure 12 shows the doping dependence of the calculated BEL rise time, *i.e.*, the time it takes for the BEL to reach 25%, 50% and 75% of its asymptotic value. The rise of the BEL to 50% of the maximum value is very fast for all doping concentrations because of extremely efficient plasmon-mediated electron-hole scatterings, whereas the ensuing increase to 75% is strongly retarded at the highest doping levels due to the increased efficiency of static screening. In contrast to the experimental results (see Fig. 4) the minimum of τ_{BEL} (for 75%) as a function of doping concentration is less pronounced, occurs at later times, and is shifted to lower doping levels. We attribute this discrepancy to the following possible causes: (*i*) additional broadening due to our incomplete description of the early thermalization stage, (*ii*) effects of electron degeneracy due to higher than nominal excitation densities which would lead to a faster BEL saturation, (*iii*) an enhancement of the DOS due to impurity banding, (*iv*) effects of hole heating at the lowest doping levels, and (*v*) impurity banding could play a minor role for the lowest doped sample and a more refined treatment of the electron-acceptor dynamics might be required for $p = 1 \times 10^{18}$ cm^{-3} [10].

However, this semiquantitative agreement between theory and experiment should not be considered as a serious drawback of our present analysis. While in this paper we have found, in particular, good agreement between theory and experiment in the low excitation regime (*i.e.*, at doping levels above 2×10^{19} cm^{-3}; see Figs. 1–3), the validity of our theoretical model in the high excitation regime (*i.e.*, at doping levels below 2×10^{18} cm^{-3}) has been proven elsewhere [10]. We conclude, that the experimental BEL alone, in comparison with theory, does not

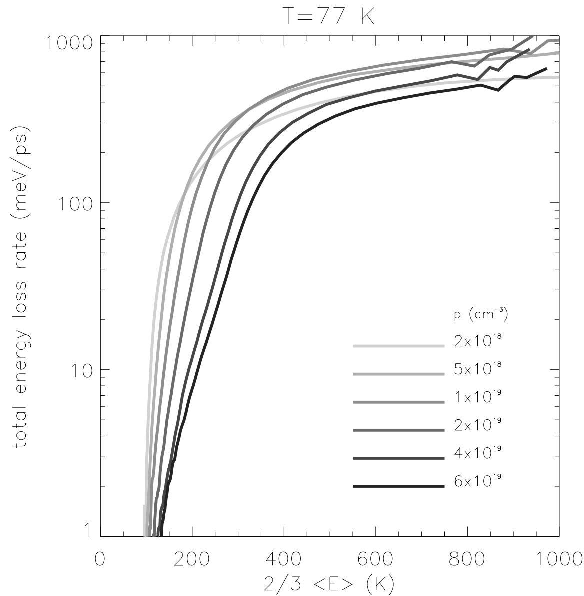

Fig. 13. Energy-loss rate as a function of electron temperature T_e for different doping levels as obtained from our EMC simulations.

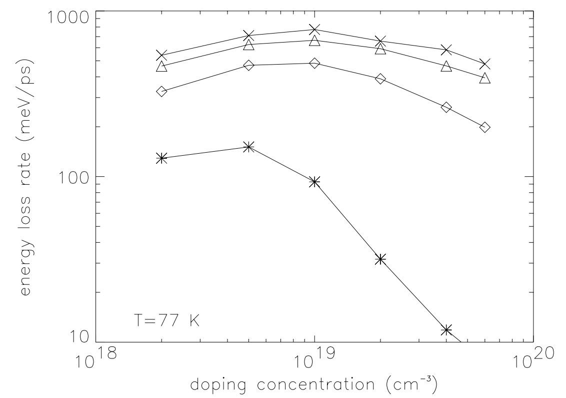

Fig. 14. Calculated energy-loss rate as a function of doping concentration for different mean electron energies 2/3 $\langle E\rangle$ = 800 K ($\times$), 600 K ($\triangle$), 400 K ($\diamond$), and 200 K ($\star$). Here the electron temperatures of 200, 400, 600, and 800 K correspond to mean electron energies of $\approx$ 26, 52, 78, and 103 meV. The densities of 0.2, 0.5, 1, 2, 4, and 6×10^{19} cm^{-3} correspond to plasmon energies of $\approx$ 26, 41, 58, 82, 115, and 141 meV.

permit a detailed quantitative measure of the energy loss. Future work should address in addition to the BEL luminescence transients at different photon energies.

4.3 Energy-loss dynamics

In contrast to the preliminary analysis of the experiments in Section 2, where an averaged energy loss was determined by use of a simplified electron-temperature model, the transient energy loss rates can be obtained *directly* from our EMC simulations. Figure 13 shows the simulated total energy-loss rate as a function of $\langle E_e\rangle$ for different doping concentrations. We observe that at high temperatures T_e the energy-loss rates can be on the order of 0.8–0.9 eV/ps. Thus, electron-hole scatterings are indeed an extremely efficient energy-loss channel for energetic minority electrons in highly p-doped semiconductors. With decreasing electron temperature the energy transfer from electrons to holes is dramatically reduced due to strong static screening by the cold background holes.

Figure 14 depicts the doping dependence of the energy-loss rates for different electron temperatures. For temperatures T_e above 400 K a maximum shows up at a doping level of $p \approx 1 \times 10^{19}$ cm^{-3}, which shifts to lower doping concentrations with decreasing T_e. This behavior can be easily understood in terms of our previous discussion about the energy-loss dynamics of one electron to a cold doping background (see Sect. 3.1), showing that the maximum of the energy-loss rate is at the density p where the mean energy is approximately twice the corresponding plasmon energy $E_{pl}(p)$. We thus conclude that the position of the maximum of $\langle\dot{E}\rangle(p)$ does not contain any signature of hole degeneracy (as one could infer from the shape of the hole-distribution functions in Fig. 8). Rather the position of the maximum relates to the present experimental conditions of an electron excess energy of $\approx$ 120 meV and a lattice temperature of 77 K. This means, in particular, that if we could go to higher excess energies and avoid the resulting transfers of photoexcited electrons to the satellite valleys of the conduction band, the maximum of the BEL rise time would shift to higher doping levels.

5 Conclusion

We have observed a maximum in the energy-loss rate of photoexcited minority electrons in highly p-doped GaAs for a doping concentration of $p \approx 2 \times 10^{19}$ cm^{-3}. Using detailed Monte-Carlo simulations we have been able to attribute this nonmonotonic behavior of the energy-loss rate as a function of doping to the transition from plasmon-mediated electron-hole scatterings at lower densities to quasistatic screening of the electron-hole scatterings by the degenerate hole plasma at high densities. This effect is observable when the excess energy of hot carriers interacting with a cold plasma is comparable to the plasmon energy and is important for understanding energy dissipation in high-density plasmas.

Our deepest thanks go to Prof. Ralph Höpfel who stimulated our interest in hot-carrier dynamics in highly doped semiconductors. Starting with his pioneering paper in 1986 [6], which reported the first observation of a negative absolute mobility of electrons in p-modulation doped GaAs quantum wells, he kept an interest in this field and constantly contributed to the frontiers of research. It has been a pleasure to have benefited from his outstanding experience and intuition. In addition, we gratefully appreciate his generous support during all stages of the present work. Ralph has always surrounded us with a friendly and stimulating atmosphere and with his cordial personality

our collaboration has been a pleasure throughout, not only scientifically but also from the personal point of view. Ralph Höpfel died under tragic circumstances on May 9th 1997 at the age of 42.

References

1. H. Elsayed–Ali, T. Juhasz, G. Smith, W.E. Bron, Phys. Rev. B **43**, 4488 (1991).
2. W.S. Fann, R. Storz, H.W. Tom, J. Bokor, Phys. Rev. Lett. **68** (1992) 2834; W.S. Fann, *et al.*, Phys. Rev. B **46**, 13 592 (1992).
3. R. Groeneveld, R. Sprik, A. Lagendijk, Phys. Rev. B **45**, 5079 (1992); *ibid.* **51**, 11 433 (1995).
4. C. Suárez, W.E. Bron, T. Juasz, Phys. Rev. Lett. **75**, 4536 (1995).
5. V.E. Gusev, O.B. Wright, Phys. Rev. B **57**, 2878 (1998).
6. R.A. Höpfel, J. Shah, P.A. Wolff, A.C. Gossard, Phys. Rev. Lett. **56**, 2736 (1986); *ibid.* **56** 765 (1986).
7. T. Furuta, A. Yoshii, Appl. Phys. Lett. **59**, 3607 (1991).
8. T. Furuta, *Semiconductors and Semimetals*, **39**, edited by R.K. Willardson, A.C. Beer (Academic Press, New York, 1993) 151.
9. A. Tomita, J. Shah, J.E. Cunningham, S.M. Goodnick, P. Lugli, S.L. Chuang, Phys. Rev. B **48**, 5708 (1993).
10. U. Hohenester, P. Supancic, P. Kocevar, X.Q. Zhou, W. Kütt, H. Kurz, Phys. Rev. B **47**, 13 233 (1993).
11. R. Rodrigues–Herzog, N.E. Hecker, R.A. Höpfel, U. Hohenester, P. Kocevar, Phys. Rev. B **55**, R7311–R7314 (1997).
12. D. Pines, *Elementary Excitations in Solids* (Benjamin, New York, 1964).
13. In p-type GaAs no significant temperature dependence of the free hole concentration has been observed in carbon-doped GaAs at $p \geq 7.2 \times 10^{18}$ cm^{-3} by H. Chen, M. Feng, M. Lin., P. Chen, C. Wu, J. Wu, J. Appl. Phys. **75**, 5453 (1994).
14. E. Schubert, *Doping in III-V semiconductors* (Cambridge University Press, New York, 1993).
15. J. Shah, *Ultrafast Spectroscopy of Semiconductors and Semiconductor Nanostructures* (Springer, Berlin, 1996).
16. Details of our experiments have been published in Ref. [11].
17. In the analysis of the experiments we calculated the bandgap renormalization according to the interpolation formula of H.J. Casey, F. Stern, Appl. Phys. Lett. **47**, 631 (1976).
18. P.C. Becker, H. Fragnito, C.B. Cruz, R. Fork, J. Cunningham, J. Henry, C. Shank, Phys. Rev. Lett. **61**, 1647 (1988).
19. H.B. Bebb, W. Williams, in *Semiconductors and Semimetals*, Vol. 8, edited by R.K. Willardson, A.C. Beer (Academic Press, New York, 1972) 181.
20. M. Sailer, Diploma Thesis, Leopold–Franzens–Universität Innsbruck, 1996.
21. T. Elsässer, J. Shah, L. Rota, P. Lugli, Phys. Rev. Lett. **66**, 1757 (1991).
22. We emphasize that in our experiments nonradiative recombination is of minor importance, as can be inferred from the long-time tail of the band-edge luminescence which stays constant over several picoseconds (see also Fig. 3).
23. R. Rodrigues–Herzog, M. Sailer, N.E. Hecker, R.A. Höpfel, N. Nintunze, M.A. Osman, Appl. Phys. Lett. **67**, 264 (1995).
24. J. Collet, Phys. Rev. B. **47**, 10 279 (1993).
25. J.R. Meyer, F.J. Bartoli, Phys. Rev. B **28**, 915 (1983).
26. C. Jacoboni, P. Lugli, *The Monte-Carlo method for semiconductor device simulation* (Springer, Berlin, 1989).
27. H.R. Trebin, U. Rössler, R. Ranvaud, Phys. Rev. B **20**, 686 (1979); we take $2\hbar^2 P^2/m_o = 23$ eV and the Luttinger parameters $\gamma_1^L = 6.85, \gamma_2^L = 2.10, \gamma_3^L = 2.90$.
28. J. Wiley, Phys. Rev. B **4**, 2485 (1971).
29. J. Young, N. Henry, P. Kelly, Solid-State Electron. **32**, 1567 (1989).
30. At this point we should shortly address the role of plasmons within the transport description of equation (2). Our use of the Boltzmann picture (*i.e.*, ballistic electrons between instantaneous energy- and momentum-conserving scattering events) describes plasmons only as virtual excitations in scattering events, whereas real plasmon processes (*i.e.*, emission and absorption of plasmons) are neglected through our restriction of solely using distribution functions as dynamic variables; see, *e.g.*, U. Hohenester, W. Pötz, Phys. Rev. B **56**, 13 177 (1997).
31. J.J. Quinn, Phys. Rev. **126** 1453 (1962).
32. T. Kuhn, F. Rossi, Phys. Rev. B **46**, 7496 (1992).
33. A. Leitenstorfer, C. Fürst, A. Lauberau, W. Kaiser, G. Tränkle, G. Weinmann, Phys. Rev. Lett. **76**, 1545 (1996).